FEBS Letters

FEBS PRESS science publishing by scientists

Cryo-EM structure of the ribosome functional complex of the human pathogen *Staphylococcus aureus* at 3.2 Å resolution

Alexander Golubev[1,2], Bulat Fatkhullin[1,3], Iskander Khusainov[1,4], Lasse Jenner[2], Azat Gabdulkhakov[1,3], Shamil Validov[1], Gulnara Yusupova[2], Marat Yusupov[1,2] and Konstantin Usachev[1]

1 Laboratory of Structural Biology, Institute of Fundamental Medicine and Biology, Kazan Federal University, Russia
2 Département de Biologie et de Génomique Structurales, Institut de Génétique et de Biologie Moléculaire et Cellulaire, CNRS UMR7104, INSERM U964, Université de Strasbourg, Illkirch, France
3 Institute of Protein Research, Russian Academy of Sciences, Puschino, Russia
4 Department of Molecular Sociology, Max Planck Institute of Biophysics, Frankfurt am Main, Germany

Correspondence
M. Yusupov and K. Usachev, Laboratory of Structural Biology, Institute of Fundamental Medicine and Biology, Kazan Federal University, 18 Kremlyovskaya, Kazan 420008, Russia
Tel: +33 (0)3 88 65 33 01
E-mails: marat.yusupov@igbmc.fr (MMIY); k.usachev@kpfu.ru (KU)

(Received 10 July 2020, revised 11 August 2020, accepted 17 August 2020, available online 10 September 2020)

doi:10.1002/1873-3468.13915

Edited by Michael Ibba

***Staphylococcus aureus* is a bacterial pathogen and one of the leading causes of healthcare-acquired infections in the world. The growing antibiotic resistance of *S. aureus* obliges us to search for new drugs and treatments. As the majority of antibiotics target the ribosome, knowledge of its detailed structure is crucial for drug development. Here, we report the cryo-EM reconstruction at 3.2 Å resolution of the *S. aureus* ribosome with P-site tRNA, messenger RNA, and 10 RNA modification sites previously not assigned or visualized. The resulting model is the most precise and complete high-resolution structure to date of the *S. aureus* 70S ribosome with functional ligands.**

Keywords: antibiotic resistance; drug targets; methyltransferases; ribosome; rRNA modifications; *Staphylococcus aureus*

Antibiotic resistance is becoming a major threat to healthcare systems around the world. A certain subset of microorganisms (ESKAPE [1] organisms) was highlighted for their tenacious and pathogenic behavior. They pose extreme threat due to their fast adaptation to drug treatment, host invasive techniques, severe outcomes for patients, and their leading role in causing hospital-acquired infections. Among these organisms, *Staphylococcus aureus* is a prominent pathogenic Gram-positive bacterium that causes acute and chronic infections with a number of highly resistant strains (such as MRSA and VRSA).

The ribosome is one of the most complex molecular machines and is one of the primary targets of antibiotics. It accomplishes the central metabolic process in living organisms—protein synthesis. The 70S bacterial ribosome is a two-subunit (large 50S and small 30S) nucleoprotein complex consisting of three strands of rRNA and 50 individual ribosomal proteins. Detailed structural data have created the foundation for mechanistic explanations of ribosome functions and the action of antibiotics. Previously, X-ray structural data of the ribosome from the model organisms *Escherichia coli* [2,3], *Thermus thermophilus* [4–8],

Abbreviations
Cryo-EM, cryogenic electron microscopy; fMet-tRNA$_i^{Met}$, formylated methionine tRNA; LSU, large subunit; PTC, peptidyl transferase center; SSU, small subunit.

Deinococcus radiodurans [9], and *Saccharomyces cerevisiae* [10] were determined at high resolution. Recently, using the advantages of cryogenic electron microscopy (cryo-EM), more organisms were added to the list such as *S. aureus* [11], *Bacillus subtilis* [12], *Plasmodium falciparum* [13,14], *Mycobacterium tuberculosis* [15], and *Pseudomonas aeruginosa* [16].

Complete and high-resolution structures of ribosomes from pathogenic bacteria, especially the species exhibiting increasing antibiotic resistance, are necessary research objects in the never-ending battle against antibiotic resistance. A series of *S. aureus* ribosome structures were investigated in the last decade—vacant 70S [11], hibernating ribosome dimers [17], and RsfS-inactivated 50S subunit [18] with antibiotics [19]. Main species-specific features such as rRNA and protein extensions were described [11]. However, the accuracy of the models and the level of detail that was achieved were limiting the interpretation of antibiotic binding sites, and better models will give new implications for structure-based drug design. Furthermore, small *S. aureus* species-specific details can be discovered using a higher resolution map.

One of the important features of ribosomes is rRNA modifications. rRNA contains many modified nucleotides in addition to the standard nucleotides. In bacteria, there are three major types of rRNA modifications: methylation of bases, methylation of ribose, and pseudouridylation. rRNA modifications broaden the chemical and structural properties of nucleotides. The specific function of a modified nucleotide does not solely stem from the chemical structure but is also based on the particular structural environment. Modifications can create a wide range of changes such as increases in structural rigidity, thermodynamics, bonding potential changes, and local base stacking enhancement, so the effects can propagate beyond the modification site [20]. rRNA modifications (see Ref. [21,22] for review) are not merely randomly distributed throughout the ribosome, but often found clustered in functional centers: the aminoacyl- (A-), peptidyl- (P-), and exit- (E-) tRNA binding sites, intersubunit bridges, and the peptidyl transferase center (PTC) [2,8,23,24]. While the exact role of each modification is not yet uncovered, the general view is that modifications are involved in proper construction of functional centers where they fine-tune ribosome functions [22]. Even though the rRNA modifications do not seem to be directly involved in the chemistry of translation, they most likely participate by stabilization of rRNA secondary and tertiary structure [25]. Modifications may stabilize otherwise unfavorable rRNA folds either by acting on the local electrostatic environment or hydrogen-bonding capacity [26]. rRNA modifications have also been implicated in ribosome assembly [21] where they may function as folding chaperones or quality control markings [27]. In bacteria, almost all rRNA modifications are made by site-specific enzymes [22]. Studies of methylation enzymes showed that deletion of a modification enzyme is rarely accompanied by a noticeable fitness loss for bacteria in non-native environments [28,29]. However, several studies have also shown that loss of some particular rRNA modifications leads to diverse negative effects: severe growth retardation [30], slower rates and accuracy of translation [31], alterations of active sites [32], and a decrease in the fidelity of translation initiation [33]. Due to recent advances in X-ray crystallography [2,8] and single-particle electron [34,35] cryo-EM, structural biology techniques have become efficient methods for verification rRNA modifications. Exceptional scientific rigor should be taken to cross-validate with biochemical and bioinformatics data if available to ensure that errors do not occur.

Particular attention has to be given to rRNA modifications in bacteria due to their role in antibiotic resistance [36]. Antibiotics targeting the ribosome often bind near or in functional centers of the ribosome where they disrupt normal ribosome function [37].

Having detailed species-specific structural data of the *S. aureus* ribosome and locations of the rRNA modifications is useful for understanding the resistance mechanisms of *S. aureus* and for the design of new antibiotics that can help in the fight against this pathogen. The data on *S. aureus* rRNA modifications and corresponding modification enzymes are very limited, and the structural data are missing. We aimed to improve the current models of the *S. aureus* ribosome with functional ligands by determining its structure at a much higher resolution than what is currently available and, thereby, create a basis that can be used in structure-based drug design. Also, we wanted to reveal the rRNA modification pattern of the *S. aureus* ribosome and correlate them to the existing data of other bacterial species.

In this study, we present the cryo-EM structure of the *S. aureus* 70S ribosome with P-tRNA and mRNA and assign 10 rRNA modifications. We correlate this information with how the modifying enzymes responsible for said modifications are conserved and possibly exploitable as potential drug targets.

Materials and methods

Staphylococcus aureus ribosome purification

70S ribosomes from *S. aureus* were obtained as described previously [11]. Two liters of *S. aureus* RN6390 culture

was grown at 37 °C in Brain Heart Infusion broth (BHI) media and harvested in early logarithmic phase. Cells were washed with buffer A (20 mM HEPES-KOH pH 7.5, 100 mM NH_4Cl, 21 mM $Mg(CH_3COO)_2$, 1 mM DTT) and pelleted, and the cell pellet was frozen at −80 °C. The cell pellet was resuspended in buffer A, supplemented with the addition of protease inhibitor cocktail (EDTA-free; Roche, Basel, Switzerland), DNase I (Roche), and lysostaphin (Sigma-Aldrich, Saint Louis, USA), and then lysed at 37 °C for 45 min. Cell debris was removed by centrifugation at 30 000 ***g*** for 90 min. The supernatant was supplemented with 2.8% w/v PEG 20 000 (Hampton Research, Aliso Viejo, USA) for fractionation. The supernatant was then recovered, and the PEG 20 000 concentration was increased to 4.2% w/v for the second fractionation. The solution was then centrifuged at 20 000 ***g*** for 10 min, and the ribosome pellet was resuspended in buffer A and layered on a sucrose cushion (10 mM HEPES-KOH pH 7.5, 500 mM KCl, 25 mM $Mg(CH_3COO)_2$, 1.1 M sucrose, 0.5 mM EDTA, 1 mM DTT). Centrifugation was subsequently carried out at 235 400 ***g*** for 15 h using a 45Ti rotor (Beckman, Brea, USA). The pellet containing ribosomes was resuspended in buffer E (10 mM HEPES-KOH pH 7.5, 100 mM KCl, 10 mM $Mg(CH_3COO)_2$, 0.5 mM EDTA, 1 mM DTT) up to a concentration of 7 $mg{\cdot}mL^{-1}$. Diluted samples were loaded onto 7–30% sucrose density gradients and centrifuged at 52 700 ***g*** for 15.5 h using a Beckman SW28 rotor. The fractions corresponding to 70S particles were pooled, and the concentration of Mg $(CH_3COO)_2$ was adjusted to 25 mM. For the sample concentrations, PEG 20 000 was added to a final concentration of 4.5% w/v. Ribosomes were pelleted by centrifugation at 20 000 ***g***, and the pellet was gently dissolved in buffer G (10 mM HEPES-KOH pH 7.5, 50 mM KCl, 10 mM NH_4Cl, 10 mM $Mg(CH_3COO)_2$, 1 mM DTT) to a final concentration of 20–25 $mg{\cdot}mL^{-1}$. Aliquots of 30 μL were flash-frozen in liquid nitrogen and stored at −80 °C.

Preparation of $tRNA_i^{Met}$

$tRNA_i^{Met}$ was prepared according to Y. Mechulam [38] with small adjustments. $tRNA_i^{Met}$ was overexpressed in *E. coli* using the plasmid pBStRNAfMetY2. The total tRNA was isolated by phenol extraction (pH 5) and then NaCl/ethanol-precipitated. Total tRNA was deacetylated in 1.8 M Tris/HCl pH 8.0 at 37 °C for 90 min and then NaCl/ethanol-precipitated. The pellet was dissolved in buffer T (20 mM Tris/HCl pH 7.5, 8 mM $MgCl_2$, 0.1 mM EDTA, 0.2 M NaCl), and $tRNA_i^{Met}$ was purified at Q Sepharose (GE Healthcare, Chicago, USA). $tRNA_i^{Met}$ was then NaCl/ethanol-precipitated, and the pellet was dissolved in mQ water. The sample was snap-frozen in liquid nitrogen and stored at −80 °C.

In vitro aminoacetylation and formylation of fMet-$tRNA_i^{Met}$

Aminoacetylation and formylation of $tRNA_i^{Met}$ were done according to references [39,40]. Briefly, $tRNA_i^{Met}$ (30 AU^{260}) was added to 1.5mL reaction mixture (30 mM imidazole-HCl pH 7.5, 100 mM KCl, 10 mM $Mg(CH_3COO)_2$, 1 mM DTT, 0.1 $\mu g{\cdot}\mu L^{-1}$ methionyl-$tRNA_i^{Met}$ synthethase (purified according to Fourmy [40]), 5 mM ATP (Thermo Fisher, Waltham, USA), 5 mM PEP (Sigma), 0.025 $mg{\cdot}mL^{-1}$ pyruvate kinase (Sigma), 80 μM methionine (Sigma), 0.1 $\mu g{\cdot}\mu L^{-1}$ methionyl-$tRNA_i^{Met}$ formyltransferase (purified according to Refs. [41,42]), prepared 0.3 mM folinic acid as a formyl donor).The reaction was incubated at 30 °C for 50 min. Reaction was stopped by adding 1/10 of volume of 20% CH_3CO_2K solution at pH 5.0. Formylated methionine tRNA (fMet-$tRNA_i^{Met}$) was phenol-extracted and precipitated by NH_4OAc–ethanol. Precipitated dry pellet was dissolved in buffer (50 mM K_3PO_4 pH 7.0, 1.7M $(NH_4)_2SO_4$), and fMet-$tRNA_i^{Met}$ was purified by hydrophobic interaction chromatography using TSK-gel Phenyl-5PW column. Pooled peak fractions of fMet-$tRNA_i^{Met}$ were buffer-exchanged into 20 mM $NH_4CH_3CO_2$ pH 5.0 and precipitated by $NH_4CH_3CO_2$/ethanol. The pellet of fMet-$tRNA_i^{Met}$ was dissolved in the final buffer (20 mM $NH_4CH_3CO_2$ pH 5.0), snap-frozen in liquid nitrogen, and stored at −80 °C.

mRNA

The mRNA used was chemically synthesized by Dharmacon (Lafayette, USA) and had the sequence: 5′-GGCAA GGAGGUAAAA**AUG**GUAAAAAAAAA-3′, which contained AUG start codon (underlined bold). mRNA was deprotected according to the manufacturer's protocol.

Staphylococcus aureus ribosome complex preparation

All components were thawed on ice. After thawing, purified *S. aureus* 70S ribosome sample was filtered through the 0.22 μm filter unit (Millipore, Burlington, USA). The *S. aureus* 70S ribosome complex was formed in the buffer G (10 mM HEPES-KOH pH 7.5, 50 mM KCl, 10 mM NH_4Cl, 10 mM $Mg(CH_3COO)_2$, 1 mM DTT). To form the complex, *S. aureus* ribosomes, at a concentration of 60 nM, were first incubated with a 2.5-fold excess of mRNA for 15 min at 37 °C and further incubated with fivefold excess of fMet-$tRNA_i^{Met}$ for 15 min at 37 °C. The complex was kept on ice until applying to grids.

Grid preparation

Four microliter of the complex (with the ribosome complex concentration of 60 nM) was applied to 400 mesh

carbon-coated holey carbon Quantifoil 2/2 grids (Quantifoil Micro Tools; glow discharge time = 30 s), blotted with filter paper from both sides for 1.5 s in a temperature- and humidity-controlled Vitrobot apparatus Mark IV (FEI, Eindhoven, Netherlands; $T = 4$ °C, humidity 100%, blot force 5, blot time 4 s, blot waiting time 30 s), and vitrified in liquid ethane precooled by liquid nitrogen.

Cryo-EM data collection

Data collection was performed on a Cs-corrector equipped Titan Krios electron microscope (FEI Company, Hillsboro, USA) at 300 kV, using the SerialEM software for automated data acquisition. Data were collected with a defocus of −1.5 to −3.3 µm at a magnification of 96 000 ***g***, giving a nominal pixel size of 1.1 Å·px^{-1}. The micrographs (7166) were recorded in super-resolution mode using Gatan K2 summit detector (Gatan Inc., Pleasanton, USA) as movie stacks resulting in pixel size 0.55 Å^2·px^{-1}. The exposure time for each movie stack was ~ 45 s, corresponding to an electron dose per frame ~ 1.5 electrons·Å^{-2} divided into 40 frames. Drift, gain corrections, and dose-weighting were performed with MotionCor2 [43] using all frames on 1x1 patches.

Data processing and map calculation

The contrast transfer function (CTF) was calculated from motion-corrected dose-weighted images using CTF [44]. After removing images having poor CTF quality (leaving a total of 6662 micrographs), ribosome particles were picked from motion-corrected and dose-weighted images in RELION 2.1 [45]. After extraction and fivefold binning (5.5 Å·px^{-1}) of 555 523 particles, reference-free 2D classification using RELION 2.1 was performed with 110 classes. After the removal of nonribosomal particles, the remaining 411 770 particles were subjected to three-dimensional (3D) classification using five classes. An initial reference model for 3D classification was generated using stochastic gradient descent (SGD) algorithm in RELION 2.1. The 3D classification was performed in two steps using 15° and 7.5° angular sampling, resulting in 127 598 selected particles that were extracted with the pixel size of 3.3 Å·px^{-1}. For further sorting, particles were sorted into four classes using focused 3D classification with a mask at the P-tRNA region. The tRNA-containing particles were unbinned to their original pixel size of 1.1 Å·px^{-1} and subjected to 3D autorefinement using the same reference as for the 3D classification job followed by postprocessing using automatic B factor estimation. The final map was estimated to be at a resolution of 3.2 Å using a FSC = 0.143 gold-standard threshold. Local resolution was estimated using RELION 2.1 [45].

Model building and validation

For model building, the 70S ribosome was extracted from the *S. aureus* vacant 70S ribosome model (PBD ID 5LI0) and P-tRNA with mRNA was extracted from the model of a *T. thermophilus* elongation complex (PBD ID 4V6F). The mRNA sequence was changed according to the sequence of mRNA used in this experiment. The obtained constructed model was rigid body fitted into our Gaussian-filtered cryo-EM density map. Initial coarse fitting of the flexible elements at the intersubunit interface and periphery was performed using phenix.real_space_refinement in Phenix [46] including simulated annealing (starting temperature = 800 K; cool rate = 100 K) and global minimization. Model and map were visually inspected in COOT [47]. Modeling of post-transcriptional modifications was performed in Coot and was based on manual analysis of the cryo-EM map of rRNAs. The densities that can be attributed to solvent molecules have been assigned as Mg^{2+} ions, and few K^+ ions were assigned based on the map signal, the alignment with initiation complex from *T. thermophilus* 70S with experimentally identified K^+ ions [48], and reasonable stereochemistry. Final minimization of coordinates was carried out in Phenix real-space refinement with default parameters. For model validation, we used the MolProbity webserver [49] and model-to-map correlation statistics from Phenix. Data and refinement statistics are summarized in Table S2.

Results and Discussion

We determined the single-particle cryo-EM structure of the *in vitro* reconstituted complex of *S. aureus* 70S bound to mRNA containing AUG start codon and Shine–Dalgarno sequence and initiator tRNA with formylated methionine residue (fMet-tRNA$_i^{Met}$) (Figs S1 and S2). The general resolution of the resulting cryo-EM map is 3.2 Å (0.143 criterion, Fig S1). In order to assess the quality of the cryo-EM map, a local resolution map was constructed [45] (Fig 1A,B). Mostly, the ribosome and functionally important parts such as the PTC and decoding center are resolved at 2.8–3.1 Å. This ensures reliable building of the atomic model and interpretation of small features such as interactions in the decoding center and rRNA modifications (Fig 1C–E and Fig S2) [83].

Ribosomal RNA modifications

Modeling and assignment of rRNA modification were based on a thorough analysis of the cryo-EM map. We are aware of the errors that may occur when assigning modifications solely based on cryo-EM maps as has been pointed out earlier [50]. To correctly assign

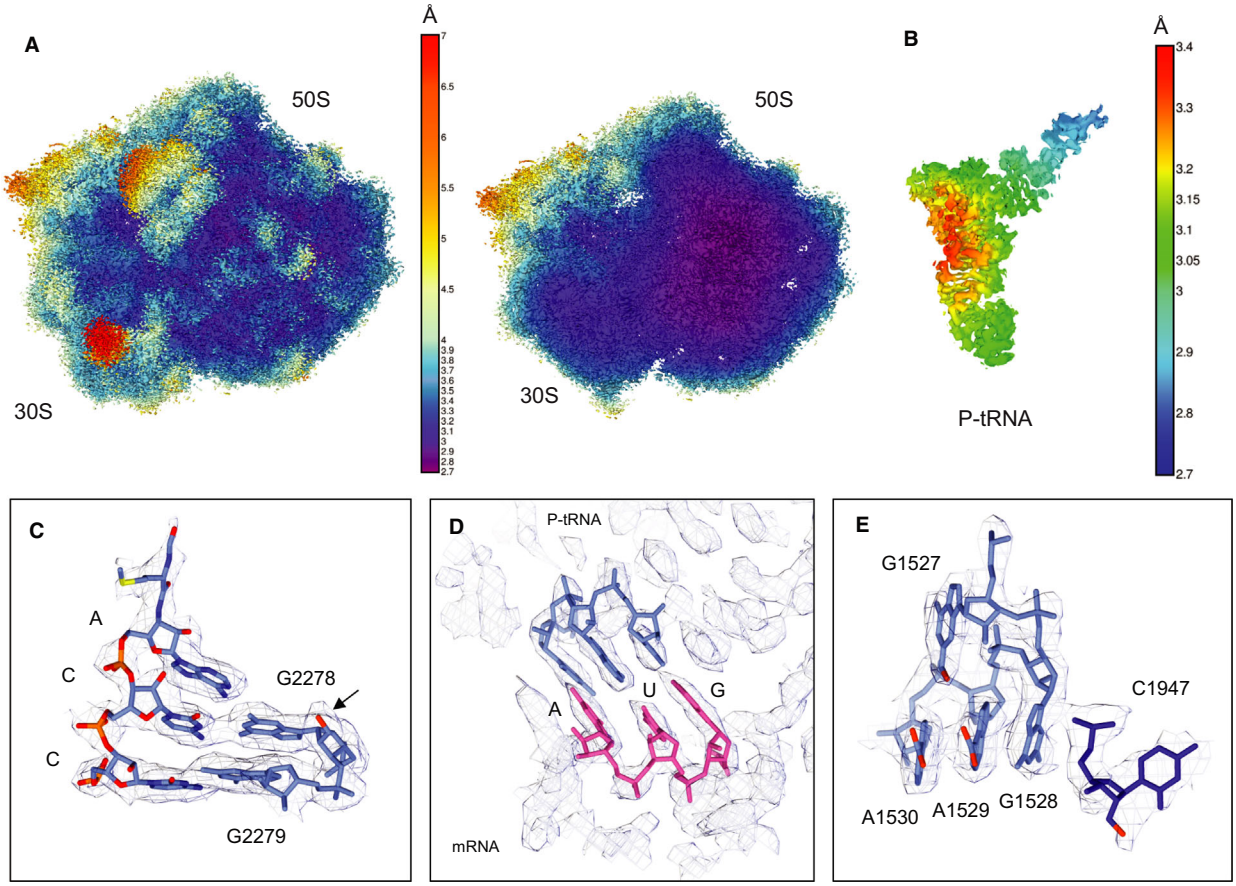

Fig. 1. Local resolution map of the *Staphylococcus aureus* cryo-EM structure. (A) Right—general overview; left—slice view through the core of ribosome. (B) Cryo-EM map of P-tRNA colored according to the local resolution. High-resolution features of the map: (C) CCA-end of P-tRNA. Modified G2278 in direct interaction with C75 of tRNA, modification is shown by orange color and arrow; (D) map quality in decoding center, AUG codon of mRNA is in magenta and P-tRNA is in blue; (E) highly modified cluster of nucleotides near the decoding center, modifications are colored in orange.

modifications, cross-correlation of data from different experimental sources is necessary. Mass spectrometry analysis of rRNA modification still comes with some limitations, and the analysis process is methodically difficult [51]; thus, the structural validation of rRNA modification is an advantage. Unfortunately, no MS data for the rRNA modifications exist for *S. aureus*. We therefore chose to cross correlate with biochemical data available from other bacterial species.

We thoroughly inspected the cryo-EM map to find places with unmodeled map density. Modifications were assigned if they were supported by the cryo-EM map and at the same time if they correlated with structurally equivalent modified positions in *E. coli* and *T. thermophilus* that have been confirmed experimentally [22]. We also used the availability of the corresponding homologous enzymes in *S. aureus* for further correlation and validation. Using this procedure, we could identify 10 sites for *S. aureus* rRNA modifications (Table 1, Figs 2 and 3) where the density allowed the confident modeling of the modified nucleotide.

In addition to the mapped modifications, we found sites, where the density map allows us to add modification, but supporting experimental data are missing. Most probably, many of the sites correspond to Mg^{2+} ions coordinated by N7 of purine nucleotides (see Fig S3G,H for two examples). However, two places—G47 of 16S rRNA and G2083 of 23S rRNA—are not coordinated by Mg^{2+} and could be possible modifications (Fig S3E,F). Additional biochemical experiments should be carried out to corroborate the results.

Modifications of 23S rRNA

We could detect sufficient density for the methyl group at 2′-O of ribose of C1947 in helix 69 (H69), despite

Table 1. Modifications of rRNA found in this study. Searches for *Staphylococcus aureus* proteins sharing similarity with known rRNA-modifying enzymes were performed using BLASTp [84]. ID of possible *S. aureus* methylases is linked to NCBI protein database.

Position in *Escherichia coli*	Position in *S. aureus*	Modification type	Location of modification	Corresponding modifying enzyme in *Escherichia coli*	Possible *S. aureus* methylase with BLAST identity percent (to *Escherichia coli* methylase if another is not stated)	Results of knockouts and information about the modification inhibition potential
23S rRNA						
–	C1947	2′-O-Methylcytidine	H69, intersubunit bridge	–	SQA11259.1 (48.36% to *Mycobacterium tuberculosis* tlyA)	*Mycobacterium tuberculosis* methyltransferase tlyA is a virulence factor and involved in hemolytic activity [54,55]
U1939	U1966	5-Methyluridine	PTC, A-site	RlmD	WP_037590442.1 28.82%	The inactivation of the *Escherichia coli* methyltransferase has mild growth effects [57,85]
G2251	G2278	2′-O-Methylguanosine	PTC, P-site	RlmB	WP_072490807 38.62%	Modification is conserved throughout all kingdoms. Deletion of RlmB in *Escherichia coli* causes slightly different phenotype from normal [28]
G2445	G2472	N2-Methylguanosine	PTC	RlmKL	WP_037588129.1 32.63% 38.76% to *Neisseria meningitidis* RlmK 32.79% to *Neisseria meningitidis* RlmL	Knockout of the methyltransferase gene reduces the growth rate of *Escherichia coli* [58]
C2498	C2525	2′-O-Methylcytidine	PTC, CCA-end of P-tRNA	RlmM	Not found	No significant growth defects [60]
A2503	A2530	2-Methyladenosine	PTC, A-site	RlmN	WP_061395092 37.79%	Modification is conserved throughout all kingdoms. PTC antibiotics susceptibility
16S rRNA						
G527	G535	N7-Methylguanosine	A-site, streptomycin binding site	RsmG	WP_025906214.1 35.58%	Improvement of growth in some conditions [86], streptomycin resistance [69,87]
C1402	C1412	N4, O 2′-Dimethylcytidine	P-site, decoding center	RsmH, RsmI	WP_156980516.1 43.96%	Modification is conserved throughout all kingdoms. Deletion of the base methylation enhances the utilization efficiency of AUU codon as an initiation codon. Mutation of cytosine in this position leads to lower growth rates [70]
A1518	A1529	N6-Dimethyladenosine	P-site, decoding center	KsgA	WP_153158791.1 34.87%	Modification is conserved throughout all kingdoms. Deficiency of the methylation restructures decoding center [32]. Deletion of methyltransferase in *Escherichia coli* decreases the fidelity of translation initiation and elongation [33], diminishes growth rates, and increases resistance to antibiotic kasugamycin that acts on translation initiation [88]

Table 1. (Continued).

Position in *Escherichia coli*	Position in *S. aureus*	Modification type	Location of modification	Corresponding modifying enzyme in *Escherichia coli*	Possible *S. aureus* methylase with BLAST identity percent (to *Escherichia coli* methylase if another is not stated)	Results of knockouts and information about the modification inhibition potential
A1519	A1530	N6-Dimethyladenosine	P-site, decoding center	KsgA	WP_153158791.1 34.87%	Modification is conserved throughout all kingdoms. Deficiency of the methylation restructures decoding center [32]. Deletion of methyltransferase in *Escherichia coli* decreases the fidelity of translation initiation and elongation [33], diminishes growth rates and increases resistance to antibiotic kasugamycin that acts on translation initiation [88]

the lack of density for the 2′-O itself. The density is not sufficiently large for it to be a Mg^{2+} ion (Fig 3B). According to the experimental model, the methylated nucleotide C1947 resides in a location of high functional importance—at intersubunit bridge region B2a, in which the loop of 23S rRNA H69 contacts helix 44 (h44) of 16S rRNA of small 30S ribosomal subunit. It was shown that H69 of large 50S ribosomal subunit acts as a regulator of decoding nucleotides in h44 of the 16S rRNA in the decoding center of the small 30S ribosomal subunit, thus is responsible for the precise conversion of genetic information into proteins [52]. Many bacteria, including *E. coli*, do not have this modification, because they do not possess the corresponding 2′-O-methyltransferase tlyA [53]. It was shown that TlyA acts as virulence factor and is likely involved in ribosome biogenesis and hemolytic activity [54–56]. Despite that inactivation of TlyA results in resistance to capreomycin and viomycin antibiotics [53], it could be a potential target for inhibition studies in *S. aureus*, due to its involvement in virulence and other major biochemical processes. The biological functions of the *S. aureus* homolog of TlyA are still largely unknown.

At a level of 1.6 σ in the density map, there is clear density indicating a methylation of U1966 at position C5 (Fig 3C). U1966 is located on the periphery of the A-site tRNA binding pocket where it can potentially interact directly with the aminoacyl end of A-site-bound tRNA. It can also indirectly influence the interactions through stabilization or destabilization of the area. In the Gram-positive bacteria *B. subtilis,* the methyltransferase RlmCD modifies both U747 and U1939 in the 23S rRNA [57], whereas this is not the case in Gram-negative bacteria like *E. coli*. Since *S. aureus* resembles *B. subtilis* more than *E. coli*, it is most likely that it also possesses a single methyltransferase. However, we observed only poor density for the possible modification at position U792 (corresponding to *E. coli* U747) and could not assign the modification at this position with high confidence (Fig S3C). The direct studies on RlmCD homolog functions in *S. aureus* could be the simplest method to discover the presence of U792 modification.

With an overall high local resolution in the area near G2278, we clearly see density for a methyl group at 2′-O of ribose of G2278 (Fig 3D). The modified G2278 is located in the PTC in the P-loop of the 23S rRNA. This nucleotide forms a direct connection with the CCA-end of P-tRNA. The modification is located on the opposite side from the binding pocket for the P-tRNA CCA-end in vicinity of the three nucleotides U2476, C2092, and A2477. The modified G2278 likely

plays a role in correct accommodation of P-tRNA, by supporting the conformation of nucleotides engaged in a base pairing. Despite the position of the modification in an important functional center, deletion of RlmB does not lead to a significantly different phenotype from the normal one [28].

Very strong density indicating the presence of a methyl group at N2 was observed for the nucleotide G2472 (Fig 3E). This modified G2472 is located in H74 of the 23S rRNA near PTC. Nucleotide G2472 forms a Watson–Crick pair with C2092 that is in very close proximity to the CCA-end of P-tRNA. The methyl group can potentially weaken hydrogen bonding between N2 of G2472 and O2 of C2092, thus indirectly influence the stability of the PTC area by prevention of base triples formation [58]. On the other side, the modification also could indirectly affect the interaction with Arg74 of the uL4 protein. In *E. coli*, enzyme RlmKL modifies both the G2445 (equivalent to *S. aureus* G2472) and G2069 [59]. In our data, we could not detect any presence of a modification at position G2096 (corresponding to G2069 in *E. coli*) possibly due to the low local resolution of the cryo-EM map in that area. Interestingly, it is possible that similar to bacteria from the genus *Neisseria*, *S. aureus* may have two separate protein homologs RlmK and RlmL corresponding to two different domains of a fusion methyltransferase RlmKL [59].

In the same region, the map clearly shows the presence of a modification at the 2′-O of C2525 ribose (Fig 3F). The modified nucleotide C2525 is buried within the peptidyl transferase loop. It interacts with A2524 that is located in proximity to protein uL16 and the CCA-end of P-tRNA. Through this interaction, the modified C2525 could possibly influence binding of P-tRNA. It is also likely that the modification could impact the position of the C2525 nucleotide and thus have an effect on the architecture of the peptidyl transferase loop. The possible importance of the modification in *S. aureus* still has to be assessed; however, deletion studies of RlmM methyltransferase that modifies C2498 in *E. coli* did not show significant effects on growth [60].

The high resolution of our data in the area around the PTC allowed us to assign the modification at A2530 (Fig 3G). This methylation even shows up in the map at very high sigma levels (2.5 σ). The modified A2530 is located in the PTC, where it creates part of the A-site binding pocket for the side chain of amino acid of A-tRNA. The modification probably enhances the stacking between nucleotides A2086 and A2530, thus likely stabilize rRNA of the PTC loop, which forms the wall of the peptide exit tunnel. Deletion of the corresponding methyltransferase YfgB/RlmN modifies translation accuracy in *E. coli* [61] and grants a minor increase in susceptibility to a number of peptidyl transferase antibiotics [62]. In clinical isolates of *E. coli*, additional methylation of A2503 by methyltransferase Cfr provides resistance to a wide range of PTC-targeting antibiotics [63,64]. In the study of Seok-Ming Toh [62], it was proposed based on experimental data that by analogy with *E. coli*, *S. aureus* should carry a methyl modification at the corresponding position A2530 of 23S rRNA, which our data corroborate.

Staphylococcus aureus possess modifying protein OrfX that is a homolog to *E. coli* YbeA that methylates 23S rRNA at position U1915 in *E. coli*, located at the end of hairpin of H69. It was previously shown that in *S. aureus*, OrfX methylates 70S ribosome [65]. According to the study, there is no effect of the loss of OrfX on bacterial fitness, growth, and oxacillin susceptibility *in vitro*. The modification at *S. aureus* U1942 (equivalent to *E. coli U*1915) is expected to be present; however, the quality of the cryo-EM map in this particular area is not of sufficient quality to allow us to assign the modification. Local resolution map at this region is around 3.1 Å, but the nucleotide is located at the periphery and thus highly flexible. YbeA activity requires prior conversion of nucleotide to pseudouridine [66], which in *E. coli* is accomplished by the pseudouridine synthase RluD that modifies three sites (Ψ1911, Ψ1915, and Ψ1917 in *E. coli*). These modified nucleotides are located at the subunit interface and interact with P- and A-site tRNAs. By inference, these nucleotides should also be modified in *S. aureus*, and due to the positional importance of this cluster, the homolog of RluD could be a suitable target for inhibition studies in *S. aureus*.

Methylation of ribose at position U2579 (U2552 in *E. coli*) is among the most conserved modifications found throughout all three kingdoms of life. This modification is located in the A-loop of 23S RNA and can influence binding of aminoacyl-tRNA to the A-site [67]. The deficiency of the corresponding modifying enzyme RlmE leads to one of the most severe phenotypes across methyltransferase knockouts in *E. coli* [68]. Since this modification is so highly conserved, it is expected to be present in the *S. aureus* ribosome; however, even though the cryo-EM density map is of quite high quality in this area, we were not able to confidently determine its presence (Fig S3B). In any case, the *S. aureus* homolog of RlmE may still represent a promising potential target for binding of inhibitors.

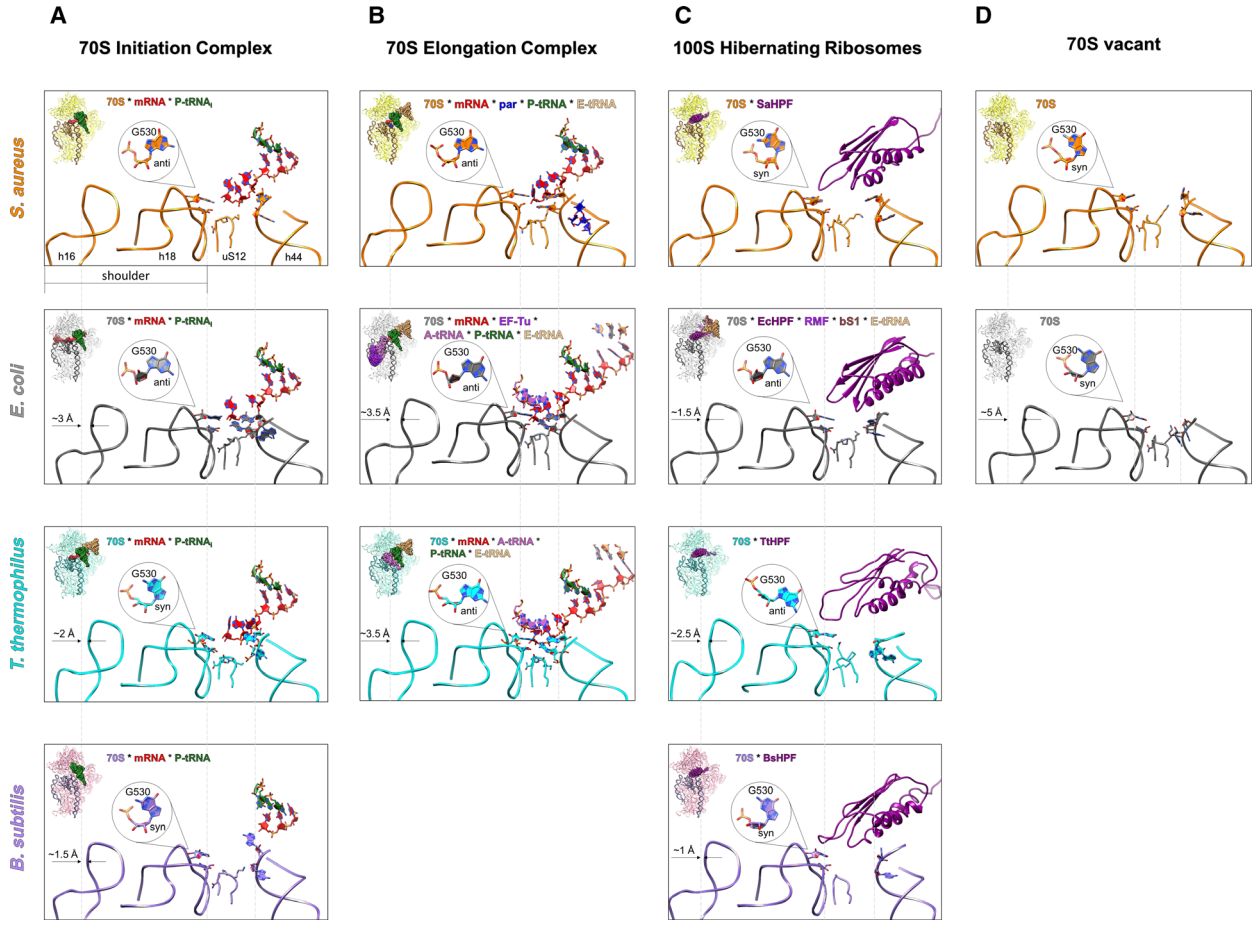

Fig. 2. Dynamics of the decoding center and shoulder position in the 70S ribosome bound to various ligands representing initiation-like state (A), elongation-like state (B), hibernation state (C), and vacant ribosome (D). Structural comparison includes representative structures of 70S from *Staphylococcus aureus* (first raw, orange ribbon), *Escherichia coli* (second raw, gray ribbon), *Thermus thermophilus* (third raw, cyan ribbon), and *B. subtilus* (fourth raw, orchid ribbon). Left-corner insets depict interface of the 30S subunits with highlighted decoding center and shoulder regions, and ligands. To measure the distances, all structures were aligned on 16S rRNA.

Modifications of 16S rRNA

The resolution of the map in the area of small 30S subunit of the ribosome allowed us to detect four modification sites. The cryo-EM map plainly shows modification at the G535 nucleotide (Fig 4B). The modified nucleotide G535 (equivalent of G527 in *E. coli*) is located in the loop of helix 18 near the A-site of the 30S subunit, close to the streptomycin binding site. The methylated nucleotide forms a Watson–Crick pair with C530, and the methyl group occupies a position near Asn59 of uS12 protein. In *E. coli*, streptomycin binds to four distinct regions of the 16S rRNA, including G526 and G527 [69], which potentially points to a role for the *S. aureus* G535 modification in acquired resistance to streptomycin.

Another modified nucleotide is located in h44 of the 16S rRNA in the heart of the P-site and directly contacts the mRNA P-codon. According to the high-resolution map in this region, C1412 holds two highly conserved modifications: 2′-O-methylation of the ribose and base methylation at N4 (Fig 4C). The methyl group at N4 directly contacts the center nucleotide of P-codon. The base methylation could also be important for the interaction of C1412 with A1511. The ribose methylation points toward the opposite site and possibly has a role in stabilization of the surrounding area. The modifications, especially the base methylation, most probably participate in the formation of the binding pocket for P-tRNA on a small subunit (SSU) and could potentially stabilize the interactions with mRNA in the P-site. Not surprisingly, it

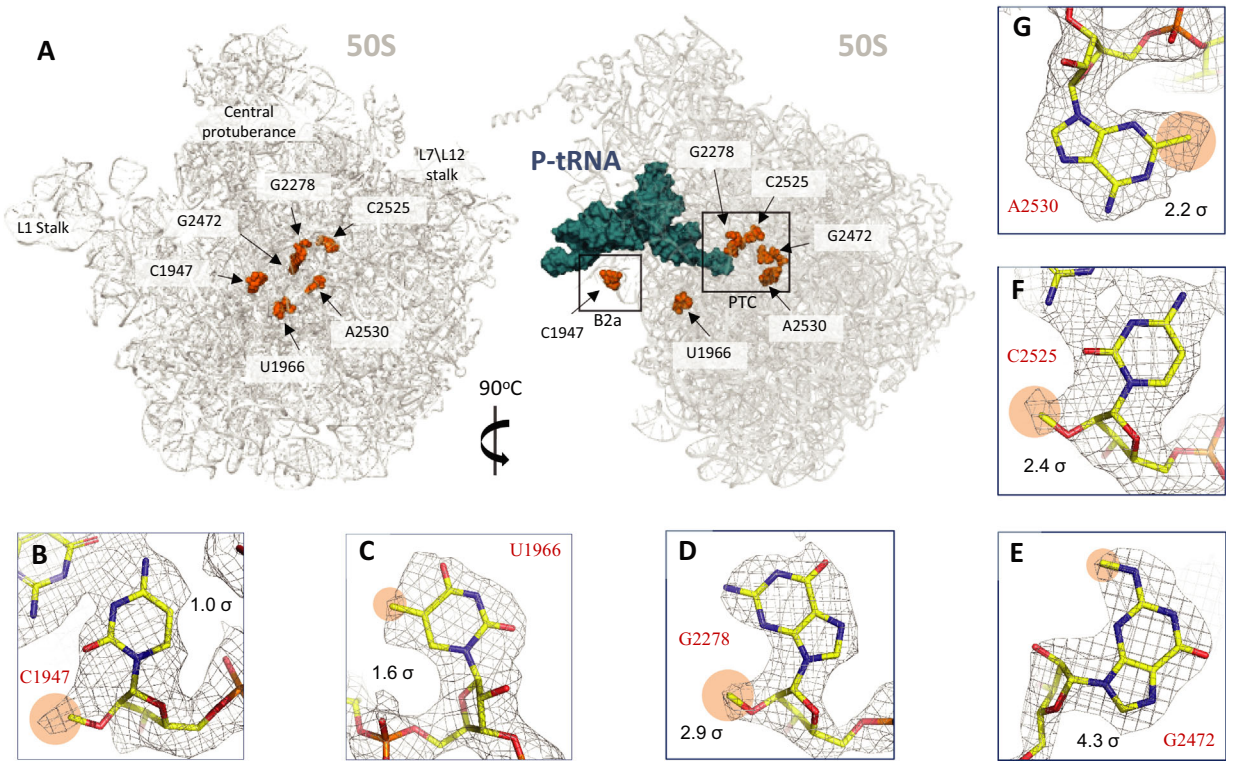

Fig. 3. Locations of modified nucleotides at LSU. (A) Locations of modified nucleotides at LSU and the map quality of assigned rRNA modifications of 23S rRNA (B–G). Modifications are shown by orange transparent circles. B2a—intersubunit bridge B2a area. LSU, large subunit.

was shown that methylations of C1402 in *E. coli* are necessary for the maintenance of the reading frame and start codon recognition [70].

In vicinity of C1412, we investigated the highly conserved modified trinucleotide loop 1527–1530 (Fig 3D–F) that is in direct contact with modified C1947 of 23S rRNA that we discussed above. We found two universally conserved dimethylated nucleotides, A1529 and A1530, which are stacking with each other (Fig 3F). They are also interacting with methylated G1527, and all these methyl modifications are clustered together. The group of nucleotides is located in h45, in close proximity to the codon–anticodon duplex between P-tRNA and mRNA, and could be involved in the formation of decoding area. In agreement with this, it was shown that the absence of these modifications restructures the decoding center [32].

One nucleotide G1527 (see Fig S3D) has the extra density appropriate for a modification, but we did not find the homologous enzyme in *S. aureus*. It is possible that in *S. aureus*, this position is modified by another enzyme (not RsmJ). The map shows extra density next to the N2 atom of the corresponding nucleotide. It has even more prominent features next to O6 and N7 atoms. Thus, we could not confidently model the modification. Supposedly, as the modified nucleotide G1527 is not highly conserved, it may play a more species-specific fine-tuning role than the dimethylated nucleotides.

The position of the modified G1207 in *E. coli* (G1189 in *T. thermophilus*) corresponds to C1217 in our *S. aureus* model. This nucleotide is located in h34 that has been implicated in translocation and decoding [71,72]. In *E. coli*, G1207 pairs with C1051 (C1051 is equivalent to G1062 in *S. aureus*). Thus, in *S. aureus* the G-C pair has been switched to a C-G pair when comparing to *E. coli* and *T. thermophilus*. The cryo-EM map clearly indicates density for possible methyl group at N2 of G1062 (Fig S3A), but since there is no other experimental nor bioinformatics data to corroborate this finding, we did not include it in the final model. *Escherichia coli* mutants with conversion of G1207 to pyrimidines have a dominant lethal phenotype [73]; therefore, the *S. aureus* functional homolog corresponding to the methyltransferase RsmC [74] responsible for the modification of G1207 in *E. coli* could be a prospective drug target.

Analysis of the functional states of the ribosomes

The resolved structure represents the 70S initiation complex formed prior to accommodation of incoming EF-Tu*tRNA complex in the A-site and contains its characteristic features such as Shine–Dalgarno and anti-Shine–Dalgarno base pairing, AUG codon–anti-codon interaction at the P-tRNA binding site, and a vacant A-tRNA binding site. The present structure expands the number of resolved states of the ribosomes from *S. aureus*, thus prompting us to perform comparative analysis of similar translational states of the ribosomes from different bacterial species. We performed such a structural comparison of the *S. aureus*, *E. coli*, *T. thermophilus*, and *B. subtilis* 70S ribosomes (a) formed with P-tRNA (initiation-like state), (b) formed with P-tRNA and A-tRNA (elongation-like state), (c) HPF-bound 70S (hibernating state), and (d) ligand-free vacant 70S ribosome (Table S1). We focused our attention on the rearrangements of the small ribosomal subunit upon transition through the given states (Fig S4). The most pronounced of them happens during accommodation of the A-tRNA. Movement of the shoulder and the head toward the body (often called 'shoulder locking' or 'domain closure') leads to stabilization of the decoding center through a network of interactions of nucleotides A1492, A1493, and G530 of 16S rRNA and Pro58 and Asn59 of uS12 protein via coordination of K^+ ions [6,48,75].

In our initiation, complex with the A-tRNA binding site is vacant, the shoulder is in an open conformation, and nucleotide 1492 is flipped into the grove of h44 and therefore in the 'in' conformation, whereas the density for nucleotide 1493 is very poor and therefore must be flexible. This is similar to what is observed for the other bacterial species in this state (Fig 2A). However, the shoulder region and more specifically the helices 16 and 18 constituting part of the shoulder region are positioned a little further away (1.5 Å for h16) from the decoding center than in *B. subtilis* and interestingly even further away (2–3 Å) than the two Gram-negative bacteria

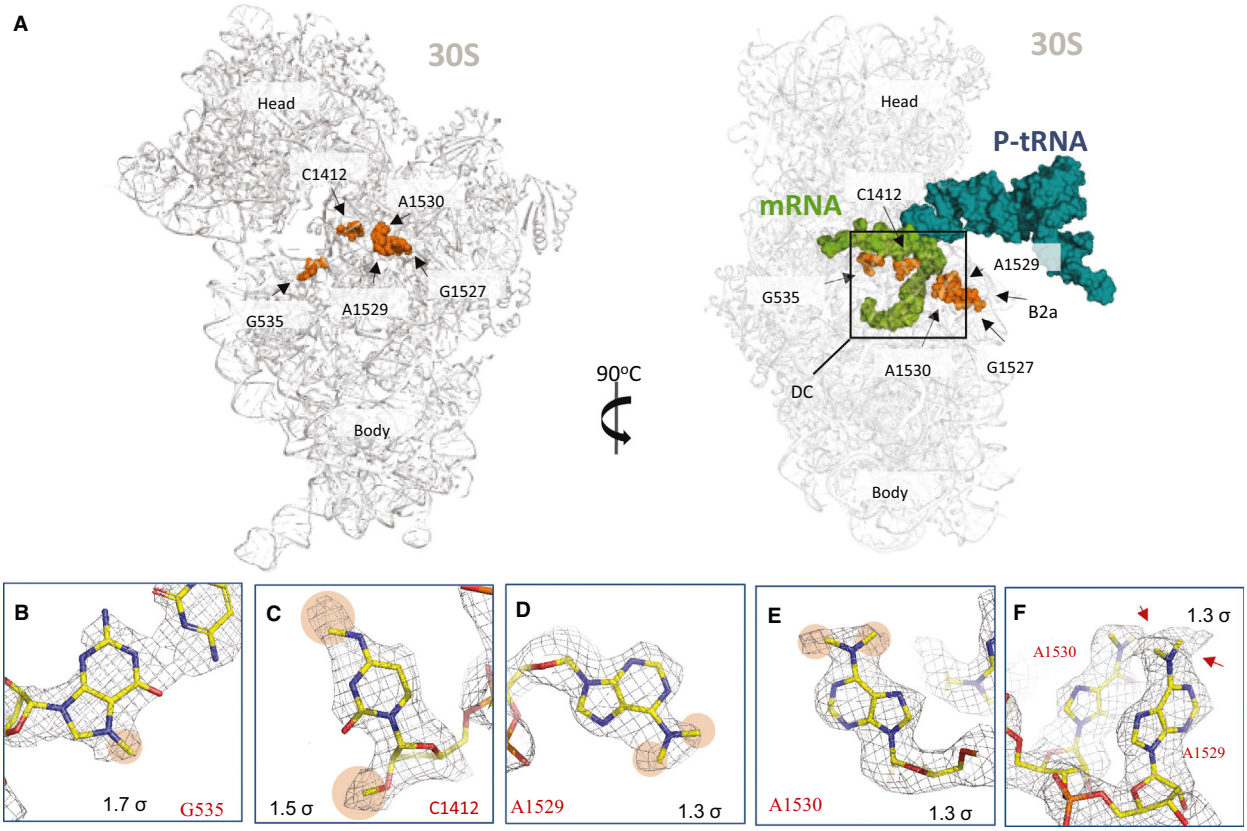

Fig. 4. Locations of modified nucleotides at SSU. (A) Locations of modified nucleotides at SS (G1527 position is shown, but it is not modified, see Sup. Picture 2 for more information) and the map quality of assigned rRNA modifications of 16S rRNA (B–F). Modifications are shown by arrows and orange transparent circles. DC—decoding center; B2a—intersubunit bridge B2a area.

T. thermophilus or *E. coli*. Interestingly, the nucleotide G530 is found in the anti-conformation in *S. aureus* and *E. coli*, whereas it is in the syn-conformation in *T. thermophilus* and *B. subtilis*. The preference for the 'anti'-conformation of G530 in the initiation state does not seem to reflect a tighter domain closure as *E. coli* and *S. aureus* have the largest difference in the distance between their shoulder region and the decoding center (Fig 2).

In the elongation state, it has been shown structurally for *T. thermophilus* [6,76–80] and *E. coli* [79,80] that accommodation of either cognate or near-cognate tRNA in the A-site of 70S leads to domain closure around the decoding center and movement of G530 to the anti-conformation if it was not there already, and A1492 and A1493 to both be in the flipped 'out' conformation. There are no structures available of the elongation state of *S. aureus*. In order to do this comparison, we therefore elected to use the structure of *S. aureus* containing the miscoding antibiotic paromomycin that known to be intercalated into the h44 and cause the flip-out conformation resulting in the stabilization of the decoding center similar to that caused by binding of A-tRNA. In all three 'elongation' complexes thus analyzed and compared, the decoding center was structurally similar, while h16 of the 30S remained in open conformation in *S. aureus* (Fig 2B). This is most probably because paromomycin alone is not capable to induce such auxiliary distant rearrangements but causes a more local reorganization. This reorganization makes the decoding center appear as if A-tRNA is already present, and thereby facilitate binding of near-cognate tRNAs explaining the error frequency increase caused by this antibiotic as previously shown [76,81]. In *T. thermophilus*, however, paromomycin was shown to favor a 30S closed conformation [75–77,82].

The open state of the 30S shoulder was also found in the hibernating 100S complexes (Fig 3C) and vacant 70S ribosome (Fig 2D). Interestingly, the conformation of the G530 nucleotide was inconsistent between the four analyzed species as illustrated in Fig 2C,D. However, for more comprehensive analysis, more structures of the identical complexes are needed to draw a reliable conclusion whether these differences are species-specific or only a result of a particular complex formation.

Conclusion

In summary, we have determined the cryo-EM structure of *S. aureus* 70S ribosome containing messenger RNA and P-tRNA at a resolution of 3.2 Å. Based on the density and existing experimental and bioinformatics data, we positively identified and assigned 10 modifications of rRNA. The present model is the highest resolution and most precise that is available at the moment. The modification sites have been thoroughly described, and possible influence on their environment and functions were proposed and correlated with existing data. Our findings indicate that at least G2278 (23S rRNA) and C1412 (16S rRNA) modifications may warrant future investigations because they are located in areas of particular interest. Due to the universal conservation of modification A2530, it also may benefit from particular scrutiny in terms of its role in antibiotic resistance. It is crucial for correct identification to perform biochemical studies of rRNA modifications in *S. aureus* (e.g., by MS analysis similar to Popova [51]), in order to be able to corroborate the existence of these modifications. We believe the proposed modifications may play an important role in protein synthesis and its regulation and, therefore, are worth investigating in greater detail.

With this study, we would like to contribute to future research on the role of rRNA modifications in *S. aureus* and their corresponding methyltransferases. Assessing the inhibition potential of the rRNA modification enzymes in *S. aureus* that we have proposed could be the way to commence exploitation of their potential to serve as general inhibition targets and targets against antibiotic resistance mechanisms. Finally, with the presented structure, we hope to accelerate structure-based drug design research on new ribosome-binding antibiotics against *S. aureus*.

Acknowledgments

The authors wish to thank IGBMC cryo-EM platform staff for helping in data collection and especially Corinne Crucifix for extensive help in grid preparation. The work was supported by the Russian Science Foundation, Grant 17-74-20009, Russia (to AGo, AGa, BF, IK, KU, SV), and cryo-EM experiments were supported by 'La Fondation pour la Recherche Médicale' DBF20160635745, France (to LJ, GY, and MMIY).

Conflict of interest

The authors declare no conflict of interest.

Data accessibility

For the cryo-EM structure of the *S. aureus*, 70S ribosome with P-site tRNA and messenger RNA

coordinates were deposited in the Protein Data Bank, PDB ID 6YEF, while the cryo-EM map was deposited in the electron microscopy database, EMD-10791.

Author contributions

AGo, IK, GY, MMIY, and KU conceived the project: AGo, IK, and SV purified 70S ribosomes under the supervision of GY and MMIY. AGo, BF, AGa, IK, and LJ refined the structures and processed the data. AGo, BF, IK, LJ, AGa, SV, and KU wrote the manuscript with input from GY and MMIY All authors revised the manuscript.

References

1 Rice LB (2008) Federal funding for the study of antimicrobial resistance in nosocomial pathogens: no ESKAPE. *J Infect Dis* **197**, 1079–1081.

2 Noeske J, Wasserman MR, Terry DS, Altman RB, Blanchard SC and Cate JH (2015) High-resolution structure of the *Escherichia coli* ribosome. *Nat Struct Mol Biol* **22**, 336–341.

3 Borovinskaya MA, Pai RD, Zhang W, Schuwirth BS, Holton JM, Hirokawa G, Kaji H, Kaji A and Cate JHD (2007) Structural basis for aminoglycoside inhibition of bacterial ribosome recycling. *Nat Struct Mol Biol* **14**, 727–732.

4 Yusupov MM, Yusupova GZ, Baucom A, Lieberman K, Earnest TN, Cate JH and Noller HF (2001) Crystal structure of the ribosome at 5.5 A resolution. *Science* **292**, 883–896.

5 Selmer M, Dunham CM, Murphy FVT, Weixlbaumer A, Petry S, Kelley AC, Weir JR and Ramakrishnan V (2006) Structure of the 70S ribosome complexed with mRNA and tRNA. *Science* **313**, 1935–1942.

6 Jenner L, Demeshkina N, Yusupova G and Yusupov M (2010) Structural rearrangements of the ribosome at the tRNA proofreading step. *Nat Struct Mol Biol* **17**, 1072–1078.

7 Jenner LB, Demeshkina N, Yusupova G and Yusupov M (2010) Structural aspects of messenger RNA reading frame maintenance by the ribosome. *Nat Struct Mol Biol* **17**, 555–560.

8 Polikanov YS, Melnikov SV, Soll D and Steitz TA (2015) Structural insights into the role of rRNA modifications in protein synthesis and ribosome assembly. *Nat Struct Mol Biol* **22**, 342–344.

9 Harms J, Schluenzen F, Zarivach R, Bashan A, Gat S, Agmon I, Bartels H, Franceschi F and Yonath A (2001) High resolution structure of the large ribosomal subunit from a mesophilic eubacterium. *Cell* **107**, 679–688.

10 Ben-Shem A, Garreau de Loubresse N, Melnikov S, Jenner L, Yusupova G and Yusupov M (2011) The structure of the eukaryotic ribosome at 3.0 A resolution. *Science* **334**, 1524–1529.

11 Khusainov I, Vicens Q, Bochler A, Grosse F, Myasnikov A, Ménétret JF, Chicher J, Marzi S, Romby P, Yusupova G *et al.* (2016) Structure of the 70S ribosome from human pathogen *Staphylococcus aureus*. *Nucleic Acids Res* **44**, 10491–10504.

12 Sohmen D, Chiba S, Shimokawa-Chiba N, Innis CA, Berninghausen O, Beckmann R, Ito K and Wilson DN (2015) Structure of the *Bacillus subtilis* 70S ribosome reveals the basis for species-specific stalling. *Nat Commun* **6**, 6941.

13 Wong W, Bai X-C, Brown A, Fernandez IS, Hanssen E, Condron M, Tan YH, Baum J and Scheres SHW (2014) Cryo-EM structure of the *Plasmodium falciparum* 80S ribosome bound to the anti-protozoan drug emetine. *Elife* **3**, e03080.

14 Sun M, Li W, Blomqvist K, Das S, Hashem Y, Dvorin JD and Frank J (2015) Dynamical features of the *Plasmodium falciparum* ribosome during translation. *Nucleic Acids Res* **43**, 10515–10524.

15 Hentschel J, Burnside C, Mignot I, Leibundgut M, Boehringer D and Ban N (2017) The Complete Structure of the Mycobacterium smegmatis 70S Ribosome. *Cell Rep* **20**, 149–160.

16 Halfon Y, Jimenez-Fernandez A, La Rosa R, Espinosa Portero R, Krogh Johansen H, Matzov D, Eyal Z, Bashan A, Zimmerman E, Belousoff M *et al.* (2019) Structure of *Pseudomonas aeruginosa* ribosomes from an aminoglycoside-resistant clinical isolate. *Proc Natl Acad Sci USA* **116**, 22275–22281.

17 Khusainov I, Vicens Q, Ayupov R, Usachev K, Myasnikov A, Simonetti A, Validov S, Kieffer B, Yusupova G, Yusupov M *et al.* (2017) Structures and dynamics of hibernating ribosomes from *Staphylococcus aureus* mediated by intermolecular interactions of HPF. *EMBO J* **36**, 2073–2087.

18 Khusainov I, Fatkhullin B, Pellegrino S, Bikmullin A, Liu W-T, Gabdulkhakov A, Shebel AA, Golubev A, Zeyer D, Trachtmann N *et al.* (2020) Mechanism of ribosome shutdown by RsfS in *Staphylococcus aureus* revealed by integrative structural biology approach. *Nat Commun* **11**, 1656.

19 Belousoff MJ, Eyal Z, Radjainia M, Ahmed T, Bamert RS, Matzov D, Bashan A, Zimmerman E, Mishra S, Cameron D *et al.* (2017) Structural basis for linezolid binding site rearrangement in the *Staphylococcus aureus* ribosome. *MBio* **8**, e03080.

20 Decatur WA and Fournier MJ (2002) rRNA modifications and ribosome function. *Trends Biochem Sci* **27**, 344–351.

21 Sergiev PV, Golovina AY, Prokhorova IV, Sergeeva OV, Osterman IA, Nesterchuk MV, Burakovsky DE, Bogdanov AA and Dontsova OA(2011) Modifications of ribosomal RNA: from enzymes to function. In

Ribosomes: Structure, Function, and Dynamics (Rodnina MV, Wintermeyer W and Green R, eds), pp. 97–110. Springer Vienna, Vienna.
22 Sergiev PV, Aleksashin NA, Chugunova AA, Polikanov YS and Dontsova OA (2018) Structural and evolutionary insights into ribosomal RNA methylation. *Nat Chem Biol* **14**, 226–235.
23 Brimacombe R, Mitchell P, Osswald M, Stade K and Bochkariov D (1993) Clustering of modified nucleotides at the functional center of bacterial ribosomal RNA. *FASEB J* **7**, 161–167.
24 Sergeeva OV, Bogdanov AA and Sergiev PV (2015) What do we know about ribosomal RNA methylation in *Escherichia coli*? *Biochimie* **117**, 110–118.
25 Sloan KE, Warda AS, Sharma S, Entian KD, Lafontaine DLJ and Bohnsack MT (2017) Tuning the ribosome: the influence of rRNA modification on eukaryotic ribosome biogenesis and function. *RNA Biol* **14**, 1138–1152.
26 Chawla M, Oliva R, Bujnicki JM and Cavallo L (2015) An atlas of RNA base pairs involving modified nucleobases with optimal geometries and accurate energies. *Nucleic Acids Res* **43**, 9573.
27 Song X and Nazar RN (2002) Modification of rRNA as a 'quality control mechanism' in ribosome biogenesis. *FEBS Lett* **523**, 182–186.
28 Lovgren JM and Wikstrom PM (2001) The rlmB gene is essential for formation of Gm2251 in 23S rRNA but not for ribosome maturation in *Escherichia coli*. *J Bacteriol* **183**, 6957–6960.
29 Pletnev P, Guseva E, Zanina A, Evfratov S, Dzama M, Treshin V, Pogorel'skaya A, Osterman I, Golovina A, Rubtsova M *et al*. (2020) Comprehensive functional analysis of *Escherichia coli* ribosomal RNA methyltransferases . *Front Genet* **11**, 97.
30 Huang L, Ku J, Pookanjanatavip M, Gu X, Wang D, Greene PJ and Santi DV (1998) Identification of two *Escherichia coli* pseudouridine synthases that show multisite specificity for 23S RNA. *Biochemistry* **37**, 15951–15957.
31 Baudin-Baillieu A, Fabret C, Liang XH, Piekna-Przybylska D, Fournier MJ and Rousset JP (2009) Nucleotide modifications in three functionally important regions of the Saccharomyces cerevisiae ribosome affect translation accuracy. *Nucleic Acids Res* **37**, 7665–7677.
32 Demirci H, Murphy F, Belardinelli R, Kelley AC, Ramakrishnan V, Gregory ST, Dahlberg AE and Jogl G (2010) Modification of 16S ribosomal RNA by the KsgA methyltransferase restructures the 30S subunit to optimize ribosome function. *RNA* **16**, 2319–2324.
33 Vanbuul CPJJ, Visser W and Vanknippenberg PH (1984) Increased translational fidelity caused by the antibiotic kasugamycin and ribosomal ambiguity in mutants harboring the Ksga gene. *FEBS Lett* **177**, 119–124.
34 Fischer N, Neumann P, Konevega AL, Bock LV, Ficner R, Rodnina MV and Stark H (2015) Structure of the *E. coli* ribosome-EF-Tu complex at <3 A resolution by Cs-corrected cryo-EM. *Nature* **520**, 567–570.
35 Coureux PD, Lazennec-Schurdevin C, Bourcier S, Mechulam Y and Schmitt E (2020) Cryo-EM study of an archaeal 30S initiation complex gives insights into evolution of translation initiation. *Commun Biol* **3**, 58.
36 Cundliffe E (1987) Ribosomal modification and resistance in antibiotic-producing organisms. *Biochem Soc Symp* **53**, 1–8.
37 Arenz S and Wilson DN (2016) Bacterial protein synthesis as a target for antibiotic inhibition. *Cold Spring Harb Perspect Med* **6**, a025361.
38 Mechulam Y, Guillon L, Yatime L, Blanquet S and Schmitt E (2007) Protection-based assays to measure aminoacyl-tRNA binding to translation initiation factors. *Methods Enzymol* **430**, 265–281.
39 Mechulam Y, Schmitt E, Maveyraud L, Zelwer C, Nureki O, Yokoyama S, Konno M and Blanquet S (1999) Crystal structure of *Escherichia coli* methionyl-tRNA synthetase highlights species-specific features. *J Mol Biol* **294**, 1287–1297.
40 Fourmy D, Mechulam Y, Brunie S, Blanquet S and Fayat G (1991) Identification of residues involved in the binding of methionine by *Escherichia coli* methionyl-tRNA synthetase. *FEBS Lett* **292**, 259–263.
41 Schmitt E, Mechulam Y, Ruff M, Mitschler A, Moras D and Blanquet S (1996) Crystallization and preliminary X-ray analysis of *Escherichia coli* methionyl-tRNA(fMet) formyltransferase. *Proteins* **25**, 139–141.
42 Schmitt E, Blanquet S and Mechulam Y (1999) Crystallization and preliminary X-ray analysis of *Escherichia coli* methionyl-tRNAMet(f) formyltransferase complexed with formyl-methionyl-tRNAMet(f). *Acta Crystallogr D Biol Crystallogr* **55**, 332–334.
43 Zheng SQ, Palovcak E, Armache JP, Verba KA, Cheng Y and Agard DA (2017) MotionCor2: anisotropic correction of beam-induced motion for improved cryo-electron microscopy. *Nat Methods* **14**, 331–332.
44 Zhang K (2016) Gctf: Real-time CTF determination and correction. *J Struct Biol* **193**, 1–12.
45 Kimanius D, Forsberg BO, Scheres SH and Lindahl E (2016) Accelerated cryo-EM structure determination with parallelisation using GPUs in RELION-2. *Elife* **5**, e18722.
46 Liebschner D, Afonine PV, Baker ML, Bunkóczi G, Chen VB, Croll TI, Hintze B, Hung LW, Jain S, McCoy AJ *et al*. (2019) Macromolecular structure determination using X-rays, neutrons and electrons:

recent developments in Phenix. *Acta Crystallogr D Struct Biol* **75**, 861–877.
47 Emsley P and Cowtan K (2004) Coot: model-building tools for molecular graphics. *Acta Crystallogr D Biol Crystallogr* **60**, 2126–2132.
48 Rozov A, Khusainov I, El Omari K, Duman R, Mykhaylyk V, Yusupov M, Westhof E, Wagner A and Yusupova G (2019) Importance of potassium ions for ribosome structure and function revealed by long-wavelength X-ray diffraction. *Nat Commun* **10**, 2519.
49 Williams CJ, Headd JJ, Moriarty NW, Prisant MG, Videau LL, Deis LN, Verma V, Keedy DA, Hintze BJ, Chen VB *et al*. (2018) MolProbity: more and better reference data for improved all-atom structure validation. *Protein Sci* **27**, 293–315.
50 Taoka M, Nobe Y, Yamaki Y, Sato K, Ishikawa H, Izumikawa K, Yamauchi Y, Hirota K, Nakayama H, Takahashi N *et al*. (2018) Landscape of the complete RNA chemical modifications in the human 80S ribosome. *Nucleic Acids Res* **46**, 9289–9298.
51 Popova AM and Williamson JR (2014) Quantitative analysis of rRNA modifications using stable isotope labeling and mass spectrometry. *J Am Chem Soc* **136**, 2058–2069.
52 Rozov A, Demeshkina N, Westhof E, Yusupov M and Yusupova G (2016) New structural insights into translational miscoding. *Trends Biochem Sci* **41**, 798–814.
53 Johansen SK, Maus CE, Plikaytis BB and Douthwaite S (2006) Capreomycin binds across the ribosomal subunit interface using tlyA-encoded 2 '-O-methylations in 16S and 23S rRNAs. *Mol Cell* **23**, 173–182.
54 Rahman MA, Sobia P, Dwivedi VP, Bhawsar A, Singh DK, Sharma P, Moodley P, Van Kaer L, Bishai WR and Das G (2015) *Mycobacterium tuberculosis* TlyA protein negatively regulates T helper (Th) 1 and Th17 differentiation and promotes tuberculosis pathogenesis. *J Biol Chem* **290**, 14407–14417.
55 Rahman A, Srivastava SS, Sneh A, Ahmed N and Krishnasastry MV (2010) Molecular characterization of tlyA gene product, Rv1694 of *Mycobacterium tuberculosis*: a non-conventional hemolysin and a ribosomal RNA methyl transferase. *BMC Biochem* **11**, 35.
56 Arenas NE, Salazar LM, Soto CY, Vizcaino C, Patarroyo ME, Patarroyo MA and Gomez A (2011) Molecular modeling and in silico characterization of *Mycobacterium tuberculosis* TlyA: possible misannotation of this tubercle bacilli-hemolysin. *BMC Struct Biol* **11**, 16.
57 Desmolaize B, Fabret C, Bregeon D, Rose S, Grosjean H and Douthwaite S (2011) A single methyltransferase YefA (RlmCD) catalyses both m(5)U747 and m(5) U1939 modifications in *Bacillus subtilis* 23S rRNA. *Nucleic Acids Res* **39**, 9368–9375.
58 Lesnyak DV, Sergiev PV, Bogdanov AA and Dontsova OA (2006) Identification of *Escherichia coli* m(2) G methyltransferases: I. The ycbY gene encodes a methyltransferase specific for G2445 of the 23 S rRNA. *J Mol Biol* **364**, 20–25.
59 Kimura S, Ikeuchi Y, Kitahara K, Sakaguchi Y and Suzuki T (2012) Base methylations in the double-stranded RNA by a fused methyltransferase bearing unwinding activity. *Nucleic Acids Res* **40**, 4071–4085.
60 Purta E, O'Connor M, Bujnicki JM and Douthwaite S (2009) YgdE is the 2'-O-ribose methyltransferase RlmM specific for nucleotide C2498 in bacterial 23S rRNA. *Mol Microbiol* **72**, 1147–1158.
61 Benitez-Paez A, Villarroya M and Armengod ME (2012) The *Escherichia coli* RlmN methyltransferase is a dual-specificity enzyme that modifies both rRNA and tRNA and controls translational accuracy. *RNA* **18**, 1783–1795.
62 Toh SM, Xiong LQ, Bae T and Mankin AS (2008) The methyltransferase YfgB/RlmN is responsible for modification of adenosine 2503 in 23S rRNA. *RNA* **14**, 98–106.
63 Arenz S and Wilson DN (2016) Blast from the past: reassessing forgotten translation inhibitors, antibiotic selectivity, and resistance mechanisms to aid drug development. *Mol Cell* **61**, 3–14.
64 Giessing AMB, Jensen SS, Rasmussen A, Hansen LH, Gondela A, Long K, Vester B and Kirpekar F (2009) Identification of 8-methyladenosine as the modification catalyzed by the radical SAM methyltransferase Cfr that confers antibiotic resistance in bacteria. *RNA* **15**, 327–336.
65 Boundy S, Safo MK, Wang L, Musayev FN, O'Farrell HC, Rife JP and Archer GL (2013) Characterization of the *Staphylococcus aureus* rRNA methyltransferase encoded by orfX, the gene containing the *Staphylococcal* chromosome cassette mec (SCCmec) insertion site. *J Biol Chem* **288**, 132–140.
66 Ero R, Peil L, Liiv A and Remme J (2008) Identification of pseudouridine methyltransferase in *Escherichia coli*. *RNA* **14**, 2223–2233.
67 Widerak M, Kern R, Malki A and Richarme G (2005) U2552 methylation at the ribosomal A-site is a negative modulator of translational accuracy. *Gene* **347**, 109–114.
68 Caldas T, Binet E, Bouloc P, Costa A, Desgres J and Richarme G (2000) The FtsJ/RrmJ heat shock protein of *Escherichia coli* is a 23 S ribosomal RNA methyltransferase. *J Biol Chem* **275**, 16414–16419.
69 Brakiergingras L and Phoenix P (1984) The control of accuracy during protein-synthesis in *Escherichia coli* and perturbations of this control by streptomycin, neomycin, or ribosomal mutations. *Canad J Biochem Cell Biol* **62**, 231–244.

70 Kimura S and Suzuki T (2010) Fine-tuning of the ribosomal decoding center by conserved methyl-modifications in the *Escherichia coli* 16S rRNA. *Nucleic Acids Res* **38**, 1341–1352.
71 Sergiev PV, Lavrik IN, Wlasoff VA, Dokudovskaya SS, Dontsova OA, Bogdanov AA and Brimacombe R (1997) The path of mRNA through the bacterial ribosome: a site-directed crosslinking study using new photoreactive derivatives of guanosine and uridine. *RNA* **3**, 464–475.
72 Kubarenko A, Sergiev P, Wintermeyer W, Dontsova O and Rodnina MV (2006) Involvement of Helix 34 of 16 S rRNA in decoding and translocation on the ribosome. *J Biol Chem* **281**, 35235–35244.
73 Jemiolo DK, Taurence JS and Giese S (1991) Mutations in 16s ribosomal-Rna in *Escherichia-coli* at methyl-modified sites - G966, C967, and G1207. *Nucleic Acids Res* **19**, 4259–4265.
74 Sunita S, Purta E, Durawa M, Tkaczuk KL, Swaathi J, Bujnicki JM and Sivaraman J (2007) Functional specialization of domains tandemly duplicated within 16S rRNA methyltransferase RsmC. *Nucleic Acids Res* **35**, 4264–4274.
75 Ogle JM, Brodersen DE, Clemons WM Jr, Tarry MJ, Carter AP and Ramakrishnan V (2001) Recognition of cognate transfer RNA by the 30S ribosomal subunit. *Science* **292**, 897–902.
76 Demeshkina N, Jenner L, Westhof E, Yusupov M and Yusupova G (2012) A new understanding of the decoding principle on the ribosome. *Nature* **484**, 256–259.
77 Rozov A, Demeshkina N, Westhof E, Yusupov M and Yusupova G (2015) Structural insights into the translational infidelity mechanism. *Nat Commun* **6**, 7251.
78 Rozov A, Demeshkina N, Khusainov I, Westhof E, Yusupov M and Yusupova G (2016) Novel base-pairing interactions at the tRNA wobble position crucial for accurate reading of the genetic code. *Nat Commun* **7**, 10457.
79 Loveland AB, Demo G and Korostelev AA (2020) Cryo-EM of elongating ribosome with EF-Tu*GTP elucidates tRNA proofreading. *Nature*, **584**, 7822: 640–645.
80 Loveland AB, Demo G, Grigorieff N and Korostelev AA (2017) Ensemble cryo-EM elucidates the mechanism of translation fidelity. *Nature* **546**, 113–117.
81 Pape T, Wintermeyer W and Rodnina MV (2000) Conformational switch in the decoding region of 16S rRNA during aminoacyl-tRNA selection on the ribosome. *Nat Struct Biol* **7**, 104–107.
82 Ogle JM, Murphy FV, Tarry MJ and Ramakrishnan V (2002) Selection of tRNA by the ribosome requires a transition from an open to a closed form. *Cell* **111**, 721–732.
83 Polikanov YS, Steitz TA and Innis CA (2014) A proton wire to couple aminoacyl-tRNA accommodation and peptide-bond formation on the ribosome. *Nat Struct Mol Biol* **21**, 787–793.
84 Altschul SF, Madden TL, Schäffer AA, Zhang J, Zhang Z, Miller W and Lipman DJ (1997) Gapped BLAST and PSI-BLAST: a new generation of protein database search programs. *Nucleic Acids Res* **25**, 3389–3402.
85 Purta E, Kaminska KH, Kasprzak JM, Bujnicki JM and Douthwaite S (2008) YbeA is the m(3)Psi methyltransferase RlmH that targets nucleotide 1915 in 23S rRNA. *RNA* **14**, 2234–2244.
86 Nichols RJ, Sen S, Choo YJ, Beltrao P, Zietek M, Chaba R, Lee S, Kazmierczak KM, Lee KJ, Wong A *et al.* (2011) Phenotypic landscape of a bacterial cell. *Cell* **144**, 143–156.
87 Okamoto S, Tamaru A, Nakajima C, Nishimura K, Tanaka Y, Tokuyama S, Suzuki Y and Ochi K (2007) Loss of a conserved 7-methylguanosine modification in 16S rRNA confers low-level streptomycin resistance in bacteria. *Mol Microbiol* **63**, 1096–1106.
88 Poldermans B, Bakker H and Vanknippenberg PH (1980) Studies on the function of 2 adjacent N-6, N-6-dimethyladenosines near the 3' end of 16-S ribosomal-Rna of *Escherichia-coli*. 4. Effect of the methylgroups on ribosomal-subunit interaction. *Nucleic Acids Res* **8**, 143–151.

Supporting information

Additional supporting information may be found online in the Supporting Information section at the end of the article.

Fig. S1. FSC curve (blue) of present Cryo-EM structure. The resolution of the Cryo-EM reconstruction is 3.2 Å according to the 0.143 criterion.

Fig. S2. (A) Map quality in the vicinity of CCA-end of fMet-tRNA$_i^{Met}$; (B) similar positions of fMet's chemical groups between the model presented in the article (in cyan) and the model with fMet-tRNA$_i^{Met}$ in pre-attack state (in magenta, PDB: 1VY4) [83]).

Fig. S3. (A) Reversed nucleotide pair in our model of *Staphylococcus aureus* compared to the *Escherichia coli* (PDB: 5AFI) model with assigned modifications. Arrow on the right shows the possible position of modification at N2 of G1063 in our model. (B, C) Highly possible modified sites with insufficient density for the modeling. (D) Questionable nucleotide G1527 with the shown modification (orange circle and model extension), arrows show prominent densities next to O6 and N7. (E, F) Possible modification sites found without biochemical experiments backup data. (G, H) Arrows show map extensions towards Mg^{2+} near N7

of purine. The sigma level is indicated for every presented map region.

Fig. S4. An overview of the 70S initiation complex model from *Staphylococcus aureus* (A). Color codes: SSU – yellow; highlighted ribosomal helices and protein uS12 – orange; large subunit – blue; mRNA – red; P-tRNA – green. (B) The 30S interface view of the complex with elements of shoulder (h16, h17), decoding center (h18, uS12) and entire h44 is highlighted in orange. (C) Close-up view at the decoding center and its respective cryo-EM density (*Escherichia coli* numbering). Nucleotides C518, G530 in anti- conformation (beige square) and the backbone of the Thr54-Leu62 loop of protein uS12 (blue square) are clearly resolved. In the absence of A-tRNA, the side chains of uS12 and nucleotide A1493 are destabilized and not well resolved in our structure, while in the P-site mRNA-tRNA base-pairing is clearly visible.

Table S1. Structural comparison of the *Staphylococcus aureus*, *Escherichia coli*, *Thermus thermophilus* and *Bacillus subtilis* 70S ribosomes.

Table S2. Data collection, refinement and validation statistics for *Staphylococcus aureus* 70S ribosome cryo-EM structure with P-site tRNA and messenger RNA.